Two-Dimensional Simulation of Wave Propagation in a Three-Pipe Junction

R. J. Pearson[1]
M. D. Bassett
P. Batten[2]
D. E. Winterbone

Department of Mechanical Engineering,
UMIST,
Manchester, England

The modelling of wave propagation in complex pipe junctions is one of the biggest challenges for simulation codes, particularly those applied to flows in engine manifolds. In the present work an inviscid two-dimensional model, using an advanced numerical scheme, has been applied to the simulation of shock-wave propagation through a three-pipe junction; the results are compared with corresponding schlieren images and measured pressure-time histories. An approximate Riemann solver is used in the shock-capturing finite volume scheme and the influence of the order of accuracy of the solver and the use of adaptive mesh refinement are investigated. The code can successfully predict the evolution and reflection of the wave fronts at the junctions whilst the run time is such as to make it feasible to include such a model as a local multi-dimensional region within a one-dimensional wave-action simulation of flow in engine manifolds.
[S0742-4795(00)01304-1]

Introduction

One-dimensional ''wave-action'' codes are now applied extensively in the design of manifolds for internal combustion engines [1–3]. Such codes can be used for the prediction of performance, turbocharger matching studies [4,5], and the calculation of noise levels radiated from the ends of the intake and exhaust systems [2,4,5]. The modelling of complex pipe junctions, however, remains a major challenge since the geometry of such junctions cannot be represented using a one-dimensional approach as these junctions often produce strong directional effects on the waves which propagate through them.

The usual assumption made at pipe boundaries is that the flow behaves in a quasi-steady manner, implying that the boundary regions are defined by infinitesimal control volumes with no mass or energy storage capacity; this means $(\partial p/\partial x) \gg (\partial p/\partial t)$. Real pipe junctions violate this criteria, most obviously in the cases of the four or five-into-one junctions in the exhaust systems of very high-performance engines. These junctions also give considerably different reflection and transmission characteristics depending on which branch of the junction a wave enters—this effect is referred to as ''directionality''. The directionality of junctions is used beneficially in ''pulse converters'' to enable several cylinders to be connected together without the waves generated by their respective blowdown pulses adversely affecting the scavenging of the other cylinders.

In order to characterize directionality effects one-dimensional ''pressure-loss'' models of junctions have been devised which require empirical data, obtained from steady flow tests, relating the pressure drop across the junction in the various directions to the pressure ratio [6–9]. Obtaining such data is extremely time consuming and the simulation model cannot be used as a design procedure since the junctions have to be manufactured before their characteristics are known. Multi-dimensional models of the unsteady flow in pipe junctions offer the prospect of removing both the need to use empirical data and the limitation of the quasi-steady assumption.

Multi-dimensional models of inviscid flows in manifolds, based on the fluid-in-cell (FLIC) method, have been used in entire engine intake manifolds [10–12]. Flamang and Sierens [13] have also illustrated that it is possible to use inviscid codes in steady-flow calculations to obtain the coefficients required by the pressure-loss models described above.

In the past 15 years major developments in numerical methods for wave propagation phenomena have produced robust and efficient numerical schemes of high accuracy [14]. In the present work an inviscid model based on a modern high-resolution shock-capturing scheme is used to simulate the propagation of shock waves in three-pipe junctions. The results are compared with corresponding schlieren images and pressure-time histories measured in the ducts. These test cases provide a rigorous examination of the capabilities of the multi-dimensional model and lay the foundations for the next phase of the work which is to ''embed'' such a model in an otherwise one-dimensional engine simulation.

Governing Equations

The governing equations of two-dimensional *inviscid* flow, in differential conservation law form are

$$\frac{\partial \mathbf{W}}{\partial t} + \frac{\partial \mathbf{F}}{\partial x} + \frac{\partial \mathbf{G}}{\partial y} = 0, \tag{1}$$

where

$$\mathbf{W} = \begin{bmatrix} \rho \\ \rho u \\ \rho v \\ \rho e_0 \end{bmatrix}; \quad \mathbf{F} = \begin{bmatrix} \rho u \\ p + \rho u^2 \\ \rho uv \\ \rho u h_0 \end{bmatrix}; \quad \mathbf{G} = \begin{bmatrix} \rho v \\ \rho uv \\ p + \rho v^2 \\ \rho v h_0 \end{bmatrix}, \tag{2}$$

and

$$e_0 = e + \tfrac{1}{2}(u^2 + v^2). \tag{3}$$

The relationships formed by substituting the elements of the **W**, **F**, and **G** vectors into Eq. (1) are the continuity, momentum (x-direction), momentum (y-direction), and energy equations, respectively. The equation set contains one more unknown than there are equations and therefore additional information is required to obtain a closure. Using the ideal gas state equation,

$$\frac{p}{\rho} = RT, \tag{4}$$

[1]Current address: Lotus Engineering, Hethel, Norfolk, England.
[2]Current address: Metacomp Technologies Inc., Westlake Village, California, USA.

Contributed by the Internal Combustion Engine Division of THE AMERICAN SOCIETY OF MECHANICAL ENGINEERS for publication in the ASME JOURNAL OF ENGINEERING FOR GAS TURBINES AND POWER. Manuscript received by the ICE Division November 5, 1998; final revision received by the ASME Headquarters May 9, 2000. Technical Editor: D. Assanis.

constrains its internal energy to be a function only of temperature of the gas and, in the special case of the fluid being a perfect gas, the internal energy and temperature are related as

$$e = c_v T. \tag{5}$$

In this equation c_v, the specific heat capacity at constant volume, is a constant.

Numerical method

Much work has been done in the last two decades on numerical methods for compressible flows [14]. Schemes based on solving a series of interface (or Riemann) problems between adjacent computational cells have largely replaced those derived purely from Taylor series expansions. Generically these schemes, based on the solution of the Riemann problem, are called Godunov-type methods [15], and introduce, in an explicit manner, the physics of wave propagation into the solution procedure.

Godunov-Type Schemes. Godunov-type schemes solve the initial value problem which evolves from the interaction of fluid states on either side of an interface. Godunov [15] supposed that the initial data in the solution domain could be replaced by a set of piecewise-constant states with discontinuities at $x_{i\pm 1/2}$ as shown in Fig. 1 for the one-dimensional case. The piecewise-constant data is taken to represent the integral average of the initial data over the interval $x_{i-1/2}$ to $x_{i+1/2}$.

The integral form of the one-dimensional Eqs. (1) becomes

$$\int_x \int_t \frac{\partial \mathbf{W}}{\partial t} + \frac{\partial \mathbf{F}}{\partial x} = 0, \tag{6}$$

where

$$\mathbf{W} = \begin{bmatrix} \rho \\ \rho u \\ \rho e_0 \end{bmatrix}; \quad \mathbf{F} = \begin{bmatrix} \rho u \\ p + \rho u^2 \\ \rho u h_0 \end{bmatrix}. \tag{7}$$

On integration this equation gives

$$(\mathbf{W}_i^{n+1} - \mathbf{W}_i^n)\Delta x + (\mathbf{F}_{i+1/2}^n - \mathbf{F}_{i-1/2}^n)\Delta t = 0, \tag{8}$$

where $\mathbf{W}$ represents the average of dependent variables for the cell shown in Fig. 2 and is given by

$$\mathbf{W}_i = \frac{1}{\Delta x} \int_{x_{i-1/2}}^{x_{i+1/2}} \mathbf{W} dx, \tag{9}$$

and $\mathbf{F}$ is the average flux across the cell boundaries over an interval of time Δt, given by

$$\mathbf{F}_{i\pm 1/2} = \frac{1}{\Delta t} \int_{t^n}^{t^{n+1}} \mathbf{F} dt. \tag{10}$$

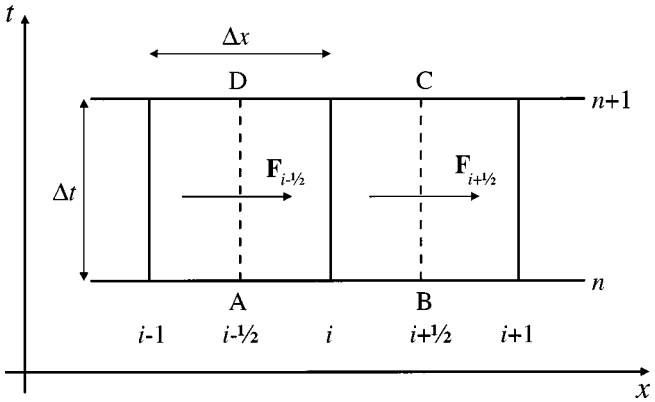

Fig. 1 Control volume for computational cell

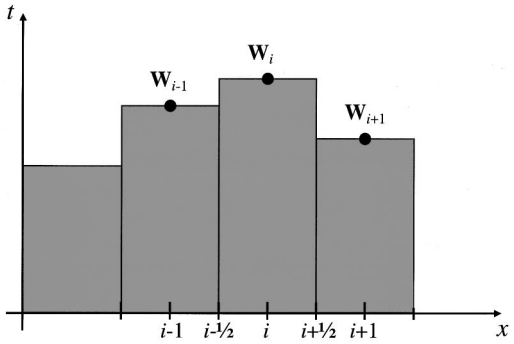

Fig. 2 Piecewise-constant reconstruction

For Godunov-type schemes the solution vector is updated by rewriting Eq. (8) as

$$\mathbf{W}_i^{n+1} = \mathbf{W}_i^n - \frac{\Delta t}{\Delta x}[\mathbf{F}_{i+1/2}^*(\mathbf{W}_i^n, \mathbf{W}_{i+1}^n) - \mathbf{F}_{i-1/2}^*(\mathbf{W}_{i-1}^n, \mathbf{W}_i^n)], \tag{11}$$

where $\mathbf{F}_{i+1/2}^*(\mathbf{W}_i^n, \mathbf{W}_{i+1}^n)$ represents the flux (10) given by the solution of the Riemann problem at $i+1/2$ formed by the piecewise-constant states in the cells at i and $i+1$.

Godunov's original method employs the exact solution to the Riemann problem [16] to find the inter-cell fluxes; this involves iterative procedures and can impose a large burden on computing resources for multi-dimensional calculations. Many ''approximate Riemann solvers'' have now emerged in the literature [14,17] which are significantly less demanding of computing time than the calculation of the exact solution. The solution method used in the present work is based on a modification, due to Toro et al. [18], of the approximate Riemann solver proposed by Harten et al. [19]. This Riemann solver reduces the computational effort required using an ''exact'' Riemann solver by approximately 40 percent.

High-Resolution Godunov-Type Schemes Using Gradient Limiters. Piecewise-constant reconstruction of the data resulting from the solution of the Riemann problem gives only first-order spatial accuracy; second-order accuracy can be obtained by using a piecewise-linear reconstruction. A straightforward approach to this linear reconstruction however, leads to the spurious oscillations which are produced by any second-order scheme with constant coefficients [17]. This problem can be overcome by the use of so-called gradient limiters [20] to modify the reconstruction so that the total variation of the reconstructed data does not exceed that of the initial data, thereby satisfying the total variation diminishing (TVD) condition [21]. This generic approach was termed MUSCL (Monotonic Upstream Scheme for Conservation Laws) by van Leer [20].

Equation (1) can be written, for an arbitrary control volume Ω, as

$$\frac{\partial}{\partial t} \int_\Omega \mathbf{W} d\Omega + \oint_S \vec{\mathbf{F}} \cdot d\vec{\mathbf{S}} = 0. \tag{12}$$

This equation asserts that the time variation of the integral averaged solution, $\mathbf{W}$, within the volume, Ω, depends only on the surface values of the fluxes. For any computational mesh with vertices ABC equation (12) can be written as

$$\frac{\partial}{\partial t} \int_\Omega \mathbf{W} d\Omega + \oint_{ABC} (\mathbf{F} dy - \mathbf{G} dx) = 0, \tag{13}$$

where $\mathbf{F}$ and $\mathbf{G}$ are the Cartesian components of the flux vector $\vec{\mathbf{F}}$ and are given in Eqs. (2). The flux across side AB of this control volume is

$$\vec{\mathbf{F}} = \mathbf{F}_{AB}(y_B - y_A) - \mathbf{G}_{AB}(x_B - x_A) = \vec{\mathbf{F}}[R_0(\mathbf{W}_L, \mathbf{W}_R)], \tag{14}$$

where $R_0(\mathbf{W}_L, \mathbf{W}_R)$ is the interface solution of the Riemann problem defined by the two interpolated states $\mathbf{W}_L$ and $\mathbf{W}_R$, either side of the interface AB. A gradient limiter is employed to ensure monotonicity of the interpolated data. In the present work a two-cycle limiter is used, which is a modified version of the scheme described by Batten et al. [22].

Results

This section describes the application of the code to the simulation of shock-wave propagation through junctions formed by the intersection of three pipes. The junction considered in this phase of the work is a 180 deg junction, where two adjacent pipes merge to become one pipe of cross-sectional area equivalent to sum of the individual pipes. A shock tube rig was constructed for the purposes of obtaining schlieren images of the waves in the junction.

Schlieren Images. Figure 3 shows the general arrangement of experimental rig developed for visualizing the density gradients (schlieren images) induced by the propagating wave. The driving tube and shock tube (pipe 1) are separated by a diaphragm which bursts when the pressure difference reaches a certain value. Since the schlieren method produces two-dimensional images the tubes were square and rectangular in section. Three piezo-resistive pressure transducers were located around the junction—one transducer in each pipe. The signal from the transducer in pipe 1 was used, via a time-delay circuit, to trigger an argon-spark-flash unit and a CCD camera. The image acquired by the CCD camera was frozen by the short duration of the light source and a sequence of images of a propagating wave front was thus constructed. This was possible because the results were found to be highly repeatable.

Figure 4 shows the schlieren image obtained 200 μs after the wave has reached the pressure transducer in pipe 1. The wave has emerged from pipe 1 in which it was propagating from left to right. On reaching the junction the wave-front expands in a more or less spherical manner (cylindrical in two-dimensions) so that it expands around the bend into pipe 3, as well as continuing in the original direction of its travel into pipe 2. A rarefaction wave is reflected backwards into pipe 1 when the shock wave encounters the area expansion formed at the pipe junction and a vortex is formed at the ''tongue''. The distortion of the wave front from a cylindrical form arises because the propagation speed in each pipe is the sum of the speed of sound and the flow velocity.

The simulated results shown in Fig. 5(*a*) were produced with the coarse mesh, using no adaptive refinement, shown in Fig. 5(*b*). The narrow cells in the center of the grid are caused by the need to represent the ''tongue'' of the junction. Clearly these density contours give a very crude depiction of the wave front. Figure 6(*a*) shows how the resolution is improved by adaptively refining the grid to the extent shown in Fig. 6(*b*); this result was achieved using approximately 11,000 cells. The grid refinement was activated when the density gradient between computational cells exceeded a given criteria.

Figures 7(*a*)–(*d*) show a schlieren image, a predicted schlieren image, and predicted density contours and velocity vectors at $t = 250$ μs. Since the schlieren system measures density *gradient* it is more appropriate to compare the measured images with the magnitude of the gradient of the density field predicted by the code, namely

$$\sqrt{\left(\frac{\partial \rho}{\partial x}\right)^2 + \left(\frac{\partial \rho}{\partial y}\right)^2}. \tag{15}$$

Figure 7(*b*) shows a predicted ''schlieren'' image of the wave system which is directly comparable with the measured image shown in Fig. 7(*a*). This was produced using a significantly higher grid refinement level than that shown in Fig. 6(*b*).

Figures 8(*a*)–(*d*) shows the schlieren image and predicted results at $t = 350$ μs. By this time the shock front has reflected from the lower wall and started to bend around the growing vortex created at the tongue of the junction. Eventually a portion of this wave-front is transmitted back into pipe 1. The vortex produced in the predicted results is due entirely to the numerical viscosity introduced by the discretization process, there being no explicit model of the fluid viscosity in the simulation. In spite of this the predicted schlieren results shown in Fig. 8(*b*) are remarkably similar to the measured schlieren image. The vortex is illustrated clearly in the velocity vectors shown in Fig. 8(*d*). At $t = 500$ μs (Fig. 9(*a*)) the vortex has detached itself from the tongue of the junction. The reflected wave from the bottom wall is just entering the mouth of pipe 1 and has reflected off the top wall of pipe 2. This situation is reliably mimicked by the simulation (Fig. 9(*b*)–(*d*)).

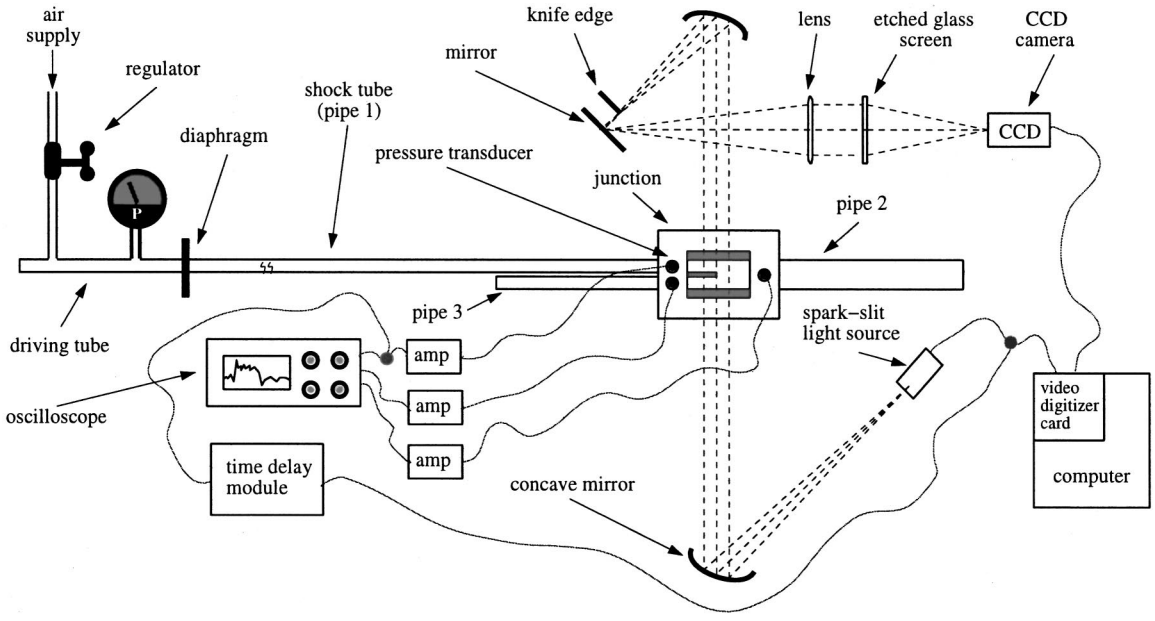

Fig. 3 General arrangement of schlieren system

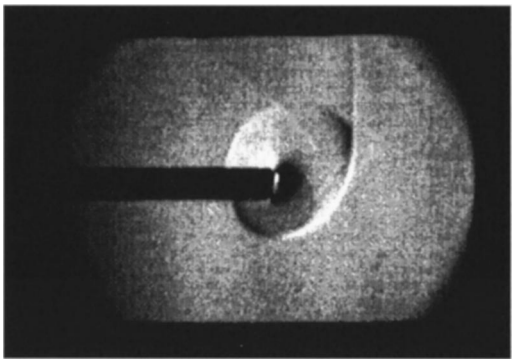

Fig. 4 Schlieren image at 200 microseconds

Numerical viscosity arises from the discretisation of the governing equations of flow and has the effect of introducing a mesh-dependent artificial mass diffusion, viscosity, and heat conduction in the continuity, momentum, and energy equations, respectively. These effects are often collectively termed ''numerical viscosity'' and are grid dependent. The focus of this paper is, however, on the modelling of the *propagation* phenomena of the waves in the pipes. The fluid flow field is driven by the pressure wave phenomena and thus the detailed flow field in the immediate vicinity of the junction is of secondary interest. It will be seen, indeed it is an aim of the paper to show, that it is possible to predict the mean pressure levels in the pipes even with an extremely coarse grid in which the fluid flow field is very poorly resolved.

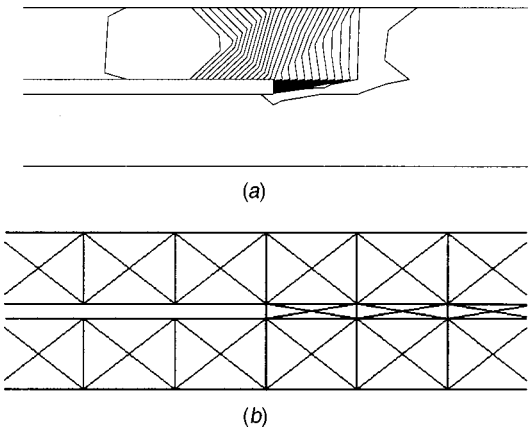

Fig. 5 (*a*) Density contours at 200 microseconds (unrefined grid); (*b*) unrefined grid

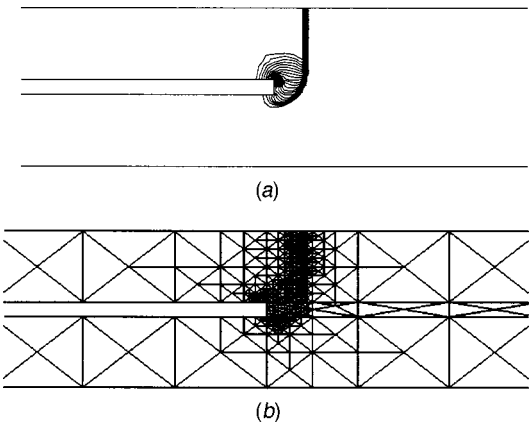

Fig. 6 (*a*) Density contours at 200 microseconds (refined grid); (*b*) refined grid at 200 microseconds

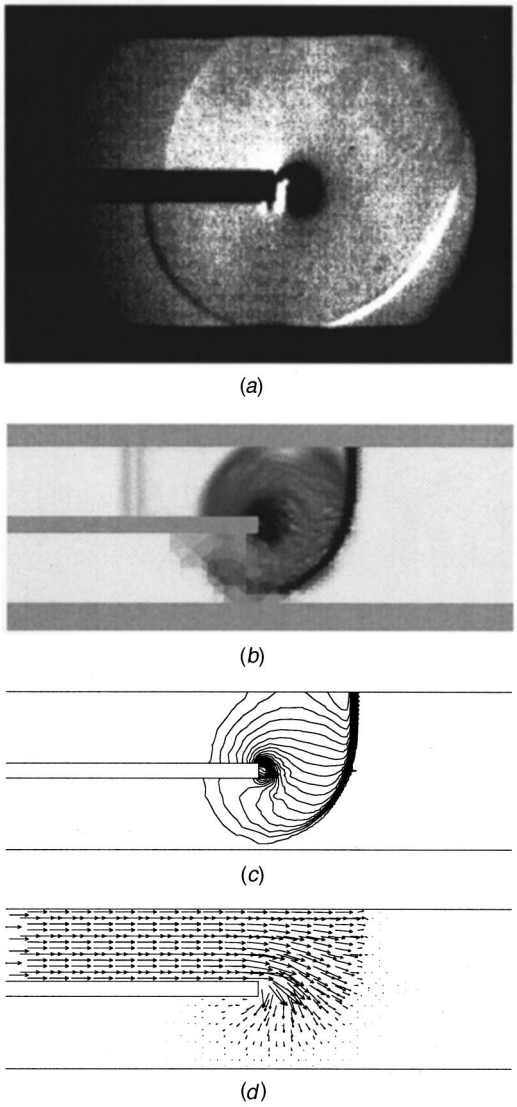

Fig. 7 (*a*) Schlieren image at 250 microseconds; (*b*) simulated schlieren image at 250 microseconds; (*c*) density contours at 250 microseconds; (*d*) velocity vectors at 250 microseconds

Pressure-Time Histories. Pressure-time histories at the transducer locations are shown in Figs. 10(*a*) and 10(*b*). It can be seen that the transmitted wave amplitude in pipe 3 is substantially smaller than both the original wave and the wave amplitude in pipe number 2. These differences in the mean level of the wave are an effect of the junction geometry on the propagation of the wave-front and it is this effect which cannot be captured directly by a one-dimensional model.

The high frequency oscillations which can be seen in the measured pressures in pipes 2 and 3 result from the transverse motion of a wave-front across the pipes. The simulation results shown in Fig. 10(*a*) predict accurately the mean levels of the transmitted pressures in pipes 2 and 3 (P2 and P3 in the diagrams). The simulated results shown in this figure were produced using an unrefined mesh of the form shown in Fig. 5(*b*). It does not seem possible to resolve the pressure caused by the transverse propagation of the waves in pipes 2 and 3 using this coarse mesh. Two predicted results are shown in each pipe, corresponding to first and second-order spatial accuracy. The results obtained using

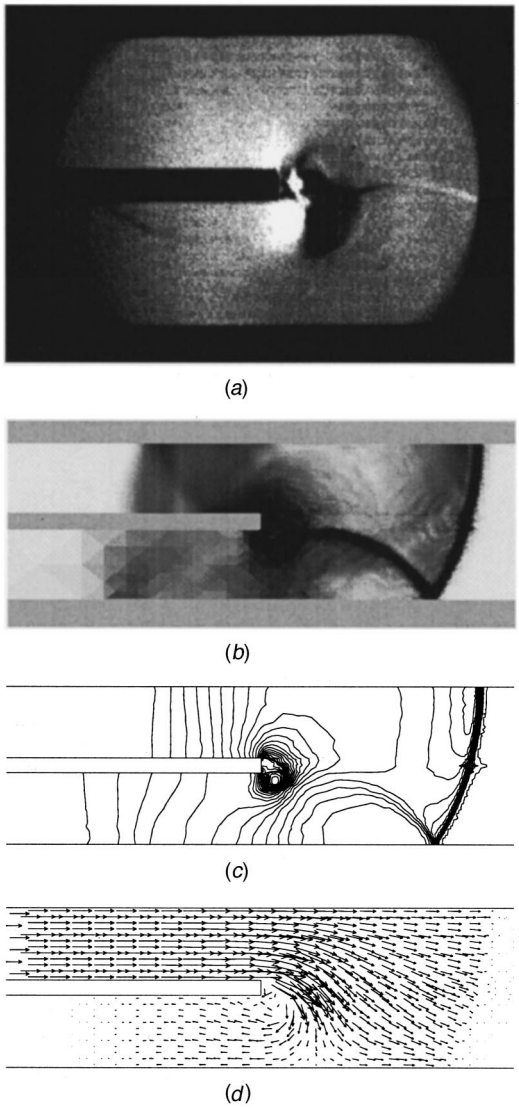

Fig. 8 (*a*) Schlieren image at 350 microseconds; (*b*) simulated schlieren image at 350 microseconds; (*c*) density contours at 350 microseconds; (*d*) velocity vectors at 350 microseconds

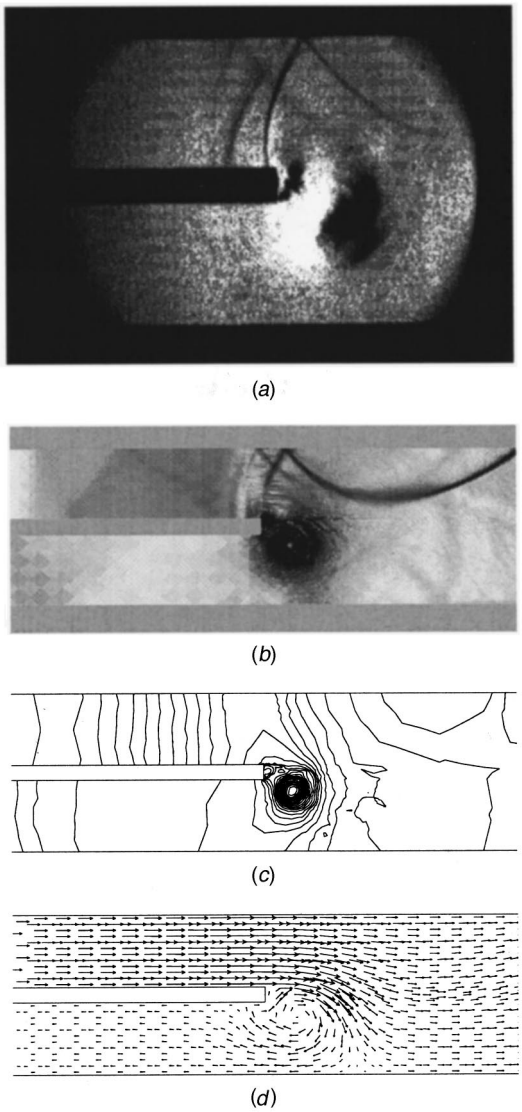

Fig. 9 (*a*) Schlieren image at 500 microseconds; (*b*) simulated schlieren image at 500 microseconds; (*c*) density contours at 500 microseconds; (*d*) velocity vectors at 500 microseconds

second-order spatial accuracy retain a steeper profile of the propagating shock waves than those produced when using first-order spatial accuracy.

Figure 10(*b*) shows that the pressure variations induced by the first three transverse wave oscillations in pipe 2 can be partially resolved by using adaptive grid refinement. An enlarged view of the pressure variation in pipe 2 is shown in Fig. 10(*c*). The shock wave gradient is significantly steeper compared with the results obtained without grid refinement. An improvement in the shock wave resolution also occurs when using first-order spatial accuracy with mesh refinement but the transverse oscillations remain unresolved.

The ability to predict the mean pressure levels of the waves propagating through the junction has a major bearing on the accuracy of volumetric efficiency predictions obtained using engine simulation programs and it is clear that the two-dimensional model used in this work affords such a facility for the square section pipes considered. The transverse component of the wave propagation would be of significance in predicting the noise spectrum radiated from the end of the pipe. However waves in engine manifolds can have wavelengths of the order of one meter or more and would thus not produce such strong transverse effects.

Wave propagation through 90 and 45 deg junctions have also been successfully simulated, as described by Pearson et al. [23] Figures 11 and 12 show measured and predicted results for a 45 deg junction with a nozzle in the pipe form which the shock emerges. Again, good correlation is obtained between the measured and predicted wave patterns (Fig. 11). After 0.3 ms the incident shock wave has propagated a significant distance away from the junction in each of the exit tubes and has reflected back from the wall opposite the entrance to the shock tube—this portion of the wave is approaching or is passing through the vortices at the exit to the shock tubes.

Figure 12 presents the pressure/time diagrams for the wave situation described in the previous area. It is clear that the nozzle in tube 1—the shock tube—has mitigated the amplitude of the pressure waves in the exit tubes. These extra losses are at the expense of having a larger pressure rise in the shock tube—indeed the pressure in the shock tube rises up to a time of 0.6 ms after the shock wave has first passed the transducer in that pipe due to the gradual reflection of a wave of increased amplitude along the nozzle-section of the junction.

Since the calculation techniques is based on a robust shock-capturing scheme the model is capable of handling much greater

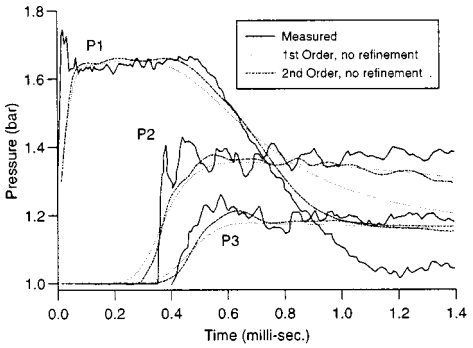

(*a*)

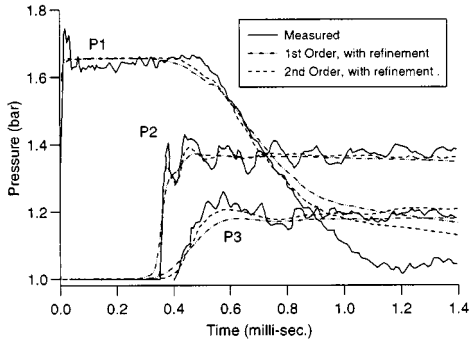

(*b*)

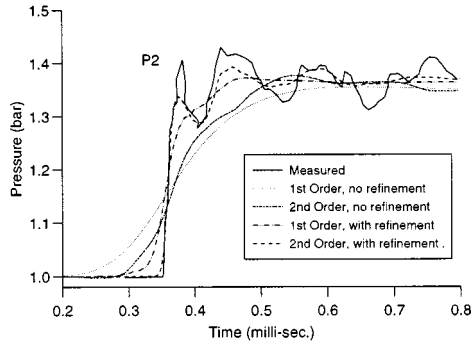

(*c*)

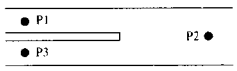

(*d*)

Fig. 10 (*a*) Pressure histories; (*b*) pressure histories; (*c*) pressure histories; (*d*) location of pressure transducers

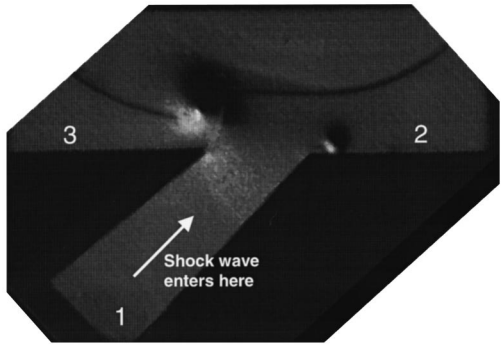

(*a*)

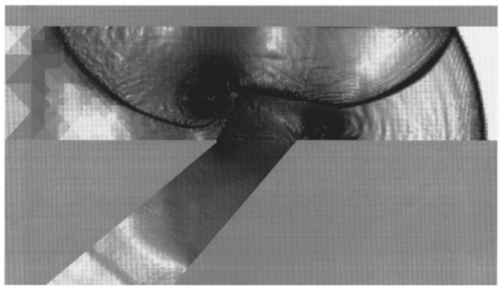

(*b*)

Fig. 11 (*a*) Schlieren image for 45 deg junction with a nozzle; (*b*) simulated schlieren image for 45 deg junction with a nozzle

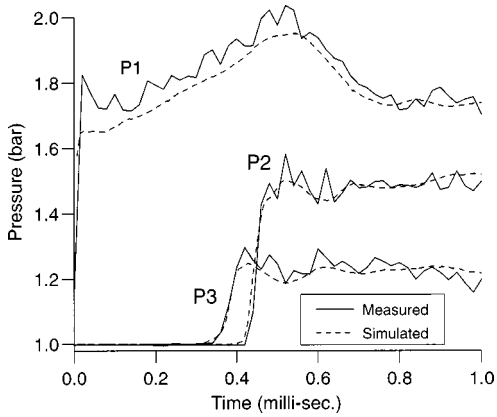

Fig. 12 Pressure histories for 45 deg junction with a nozzle

wave strengths than those used in the present work. Results for pressure ratios of 4 to 1 are shown by Batten et al. [22] and the code has been tested with much stronger waves.

Run Time. The computing time required for a simulation of duration 0.002 s after the wave has passed the first transducer location, in a domain containing 280 triangles, and using no grid refinement, is 14.0 seconds on a Silicon Graphics O2 workstation (180 MHz, 64 MB RAM). When adaptive grid refinement is used, producing a maximum of 646 triangles, the computing time increases to 52.2 s. In both cases quoted second-order spatial accuracy was used.

On the same computer 106.9 s CPU time was required to model five cycles of operation of a naturally aspirated four-cylinder spark-ignition engine using a comprehensive engine simulation program with a one-dimensional calculation of the manifold gas dynamics (using a centred-difference scheme with a flux limiter and 220 computational cells). Since the engine speed for this case was 3000 rev/min this represents a duration of 0.2 seconds. Hence the two-dimensional model of a three-pipe junction (no adaptive grid refinement) requires about 13 times as much computational effort as a typical simulation of a complete engine using a one-dimensional program with a simple two-zone combustion model.

Conclusions

It has been established that a two-dimensional inviscid model can predict the correct transmitted pressure levels when a shock wave encounters a simple three-pipe junction. Figures 5 and 6 show that it is not necessary to use a fine mesh in order to predict the mean pressure levels in the ducts. Indeed this can be achieved with a much coarser mesh than is required to produce well resolved two-dimensional images of the wave front. Hence, the pressure-loss characteristics of the junction can be modelled with a very simple representation of the boundary. It is therefore an-

ticipated that the use of such a model as a local multi-dimensional region in a one-dimensional simulation of gas dynamics in engine manifolds will not require unacceptably large computing resources.

Acknowledgments

The authors are grateful for financial support for this project from EPSRC and the Ford Motor Company. The authors are indebted to Mr. E. Clough, Dr. H. Frost, and Mr. R. Lever for assistance with the experimental work undertaken in this project.

Nomenclature

e = specific internal energy
e_0 = specific stagnation internal energy
$\mathbf{F}$ = vector of flux terms
h_0 = specific stagnation internal energy
p = pressure
R = specific gas constant
t = time
T = temperature
u = velocity
$\mathbf{W}$ = state vector
x = distance
ρ = density

References

[1] Bensler, H. P., and Oppermann, R., 1996, ''CFD Optimization of Powertrain Components,'' *I. Mech. E. Third International Conference on Computers in Reciprocating Engines and Gas Turbines*, 9–10 January.
[2] Wren, C. S., and Johnson, O., 1995, ''Gas Dynamic Simulation for the Design of Intake and Exhaust Systems—Latest Techniques,'' SAE Paper 951367.
[3] Bazari, Z., Smith, L. A., Banisoleiman, K., and French, B., 1996, ''An Engineering Building Block Approach to Engine Simulation With Special Reference to New Application Areas,'' *Third International Conference on Computers in Reciprocating Engines and Gas Turbines*, 9–10 January.
[4] Ferrari, G., and Onorati, A., 1994, ''Determination of Silencer Performances and Radiated Noise Spectrum by 1-D Gas Dynamic Modelling,'' Paper no. 945135, XXV FISITA Congress, Beijing, China.
[5] Payri, F., Torregrosa, A. J., and Broatch, A., 1997, ''A Numerical Study of the Study of a Turbocharged Diesel Engine as a Noise Source,'' SAE Paper 970836.
[6] Benson, R. S., Woollatt, D., and Woods, W. A., 1963–64, ''Unsteady Flow in Simple Branch Systems,'' *Proc. I. Mech. E.*, **178**, pp. 3–28.
[7] Watson, N., and Janota, M. S., 1971, ''Non-Steady Flow in an Exhaust System With a Pulse Converter,'' *Proc. I. Mech. E., Fluid Mechanics Conference*, Salford.
[8] Winterbone, D. E., Nichols, J. R., and Alexander, G. I., 1985, ''The Evaluation of the Performance of Exhaust Systems Equipped With Integral Pulse Converters,'' *16th Int. CIMAC*, Oslo, June.
[9] Chan, C. L., Winterbone, D. E., Nichols, J. R., and Alexander, G. I., 1986, ''A Detailed Study of Compact Exhaust Manifolds Applied to Automotive Diesel Engines,'' *Proc. Instn. Mech. Engrs. Conf.: Turbocharging and Turbochargers*, Paper No. C113/86, pp. 269–281.
[10] Tosa, Y., Shimoda, K., and Oikawa, H., 1985, ''Calculation of 2-Dimensional Unsteady Flows in Inlet Pipe System and Its Application for V-8 Resonant Intake System'', *ASME Conf. on Flows in Internal Combustion Engines—III*, Miami, pp. 63–70.
[11] Zhao, Y., and Winterbone, D. E., 1991, ''Numerical Simulation of Multi-Dimensional Flow and Pressure Dynamics in Engine Intake Manifolds,'' *Instn. Mech. Engrs. International Conf., Computers in Engine Technology*, Cambridge, Sept. 10–12.
[12] Zhao, Y., and Winterbone, D. E., 1994, ''A Study of Multi-Dimensional Gas Flow in Engine Manifolds,'' *Proc. Instn. Mech. Engrs.*, Part D, **208**, pp. 139–145.
[13] Flamang, P., and Sierens, R., 1989, ''Experimental and Theoretical Analysis of the Flow in Exhaust Pipe Junctions,'' *Proc. Instn. Mech. Engrs.*, Paper No. C382/082, pp. 461–468.
[14] Toro, E. F., 1997, *Riemann Solvers and Numerical Methods for Fluid Dynamics*, Springer-Verlag, New York.
[15] Godunov, S. K., 1959, ''A Finite Difference Method for the Numerical Computation of Discontinuous Solutions of the Equations of Fluid Dynamics,'' Math. Sbornik, **47**, pp. 271–306.
[16] Sod G. A., 1978, ''A Survey of Several Finite Difference Methods for Systems of Non-Linear Conservation Laws,'' J. Comput. Phys., **27**, pp. 1–31.
[17] Hirsch, C., 1990, *Numerical Computation of Internal and External Flows*, **2**. Wiley, Chichester.
[18] Toro, E. F. Spruce, M., and Speares, W., 1994, ''Restoration of the Contact Surface in the HLL-Riemann Solver,'' Shock Waves, **4**, pp. 25–34.
[19] Harten, A., Lax, P. D., and van Leer, B., 1983, ''On Upstream Differencing and Godunov-Type Schemes for Hyperbolic Conservation Laws,'' SIAM Rev., **25**, No. 1, pp. 35–61.
[20] van Leer, B., 1979, ''Towards the Ultimate Conservative Difference Scheme V. A Second-Order Sequel to Godunov's Method,'' J. Comput. Phys., **32**, pp. 101–136.
[21] Harten, A., 1983, ''High Resolution Schemes for Hyperbolic Conservation Laws,'' J. Comput. Phys., **49**, pp. 357–393.
[22] Batten, P., Lambert, C., and Causon, D., 1996, ''Positively Conservative High-Resolution Convection Schemes for Unstructured Elements,'' Int. J. Numer. Methods Eng., **39**, pp. 1821–1838.
[23] Pearson, R. J., Bassett, M. D., Batten, P., Winterbone, D. E., and Weaver, N. W. E., 1999, ''Multi-Dimensional Wave Propagation in Pipe Junctions,'' SAE Paper 1999-01-1186.